Imprinting Skyrmion spin textures in spinor Bose–Einstein condensates

2012 New J. Phys. 14 053013

(http://iopscience.iop.org/1367-2630/14/5/053013)

New Journal of Physics
The open-access journal for physics

Imprinting Skyrmion spin textures in spinor Bose–Einstein condensates

Jae-yoon Choi[1,2], Woo Jin Kwon[1,2], Moonjoo Lee[1,2], Hyunseok Jeong[1], Kyungwon An[1] and Yong-il Shin[1,2,3]

[1] Department of Physics and Astronomy, Seoul National University, Seoul 151-747, Korea

[2] Center for Subwavelength Optics, Seoul National University, Seoul 151-747, Korea

E-mail: yishin@snu.ac.kr

New Journal of Physics **14** (2012) 053013 (11pp)
Received 23 December 2011
Published 9 May 2012
Online at http://www.njp.org/
doi:10.1088/1367-2630/14/5/053013

Abstract. We investigate an experimental method for imprinting Skyrmion spin textures in a spinor Bose–Einstein condensate by rapidly moving the zero-field center of a three-dimensional (3D) quadrupole magnetic field through the condensate. Various excitations such as 2D Skyrmions and coreless vortices were created in spin-1 sodium condensates, initially prepared in a uniform polar or ferromagnetic phase. The spin textures were characterized with the spatial distribution of the spin tilt angle, which is found to be in good quantitative agreement with the local description of single spins under the field rotation. We demonstrate the creation of a highly charged Skyrmion in a trapped condensate by applying the imprinting process multiple times.

[3] Author to whom any correspondence should be addressed.

Contents

1. Introduction **2**
2. Spin texture imprinting by spin rotation **3**
2.1. Spin tilting by B-field rotation 3
2.2. Skyrmion spin texture with a quadrupole magnetic field 4
2.3. The polar phase versus the ferromagnetic phase of spin-1 condensates 4
3. Experimental results **5**
3.1. The creation of Skyrmion spin textures in trapped condensates 5
3.2. Characterization of the spin texture imprinting method 6
3.3. The creation of highly charged Skyrmions 7
4. Summary and outlook **8**
Acknowledgments **9**
References **9**

1. Introduction

Topological excitations play a central role in describing the physics of ordered mediums such as superfluid helium, liquid crystals and atomic Bose–Einstein condensates. In particular, Bose–Einstein condensates of atoms with internal spin degrees of freedom provide unique opportunities for the study of topological excitations. The rich structure of their order parameters can host various topological objects [1–5], and well-developed manipulation techniques for atomic motion and spin states enable us to engineer topological states of interest for investigating their dynamics and stability in a highly controllable manner. Quantized vortices have been created in single- or multi-component condensates by external rotation [6] and phase imprinting methods [7–9], leading to the successful study of their many interesting phenomena such as line defect deformation [10], Tachenko's modes in vortex lattices [11], vortex dipole dynamics [12, 13] and dynamical instability of doubly charged vortices [14]. Recently, coreless vortex states with Skyrmion spin textures were created in spinor condensates by using spatially tailored magnetic field rotation [15] or optical Raman transitions [16].

In this paper, we investigate the magnetic field rotation method for imprinting Skyrmion spin textures in a spinor Bose–Einstein condensate. The Skyrmion spin texture is characterized by a local spin that is continuously inverted to the opposite direction from a uniform spin texture. In our experiments, this spin texture is imprinted by rapidly moving the zero-field point of a three-dimensional (3D) quadrupole magnetic field through a trapped spin-1 condensate, creating 2D Skyrmions and coreless spin vortices in a polar phase and the Anderson–Toulouse and Mermin–Ho vortex states in a ferromagnetic phase. We analyze the spatial structure of the created spin textures and find that the tilt angle of spins is quantitatively well described by the local field rotation, showing that the effects due to atom–atom interactions are not involved in our spin texture imprinting process. This observation allows us to propose a scheme with multiple applications of the imprinting process and we demonstrate the creation of a highly charged Skyrmion in a trapped condensate.

In section 2, we present a brief theoretical description of the imprinting method and introduce various excitations with the Skyrmion spin texture in spin-1 condensates. Section 3 shows the experimental results and the quantitative analysis of the spatial distribution of the

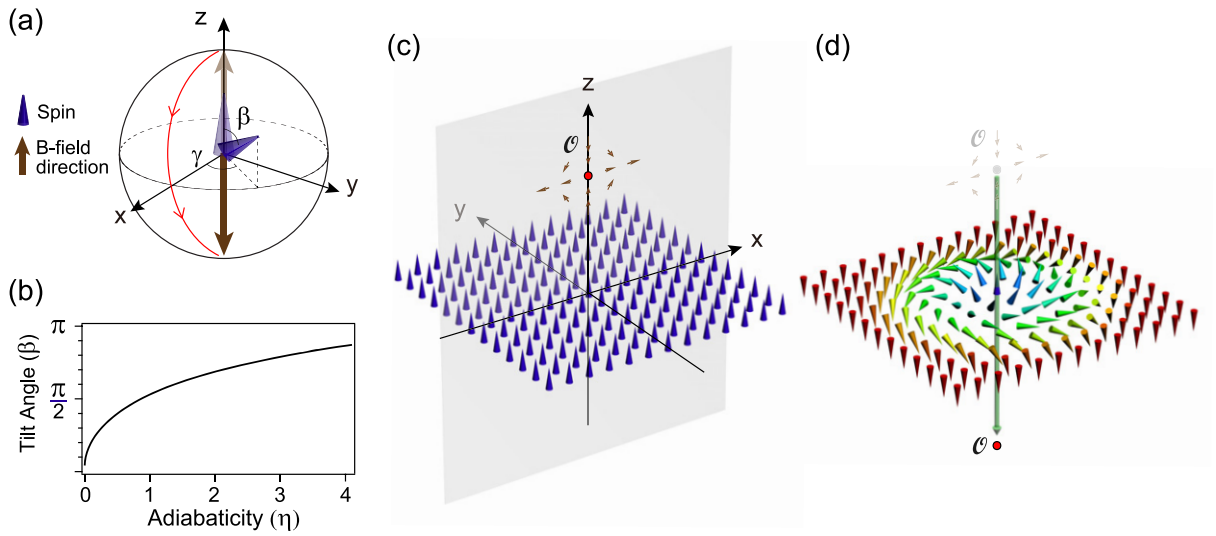

Figure 1. Spin texture imprinting by magnetic field rotation. (a) A spin, initially aligned to the $+z$-direction, tilts under magnetic field rotation (arrowed red line). (b) Numerical results for the final tilt angle β as functions of the adiabaticity η of the field rotation process (see the text for details). (c,d) Imprinting a Skyrmion spin texture with a 3D quadrupole magnetic field. As the zero-field point $\mathcal{O}$ penetrates through a 2D spinor condensate, each atomic spin experiences local magnetic field rotation, resulting in a Skyrmion spin texture. The direction of a local spin is indicated by an arrowhead, colored as its tilt angle to the z-axis.

spin tilt angle in the spin textures. Finally, in section 4 we demonstrate an experimental scheme for creating highly charged Skyrmion spin textures with two consecutive applications of the imprinting process to a trapped condensate.

2. Spin texture imprinting by spin rotation

2.1. Spin tilting by B-field rotation

The motion of a spin in a time-dependent, external magnetic field $\vec{B}(t)$ is governed by

$$\frac{\mathrm{d}\vec{s}}{\mathrm{d}t} = \frac{g\mu_\mathrm{B}}{\hbar}\vec{s} \times \vec{B}(t), \tag{1}$$

where $\vec{s}$ is a unit vector for the spin direction, g is the g-factor of the spin, μ_B is the Bohr magneton and $\hbar$ is the Planck constant h divided by 2π. The spin precesses around the axis of the magnetic field with the Larmor frequency $\omega_\mathrm{L} = g\mu_\mathrm{B}|\vec{B}|/\hbar$ and the precession axis of the spin is dragged to the field direction when the direction of the magnetic field changes. If the changing rate of the field direction $\omega_\mathrm{B} = \frac{\vec{B}}{|\vec{B}|^2} \times \frac{\mathrm{d}\vec{B}}{\mathrm{d}t}$ is much lower than the Larmor frequency, the spin adiabatically follows the magnetic field, i.e. preserving its angle from the field direction. On the other hand, if the field direction changes relatively rapidly, the angle evolves dynamically, i.e. inducing diabatic population transfer between the magnetic sublevels of the spin.

Let us consider the situation depicted in figure 1(a) where the spin is initially aligned to the $+z$-direction and the external magnetic field rotates from $+\hat{z}$ to $-\hat{z}$ as $\vec{B}(t) = B_0\hat{x} + B_z(t)\hat{z}$ with

linearly sweeping $B_z(t)$ from $+\infty$ to $-\infty$. With $B_0 = 0$, the magnetic field suddenly changes its direction to the opposite one, so the spin is not affected and keeps pointing to the $+z$-direction. On the other hand, when $B_0 \gg 1$, the spin adaptively follows the rotating field and ends up pointing in the $-z$-direction. We numerically calculate the final tilt angle β of the spin from the z-axis after the field rotation and show the result in figure 1(b) as a function of $\eta = \min(\omega_L/\omega_B) = g\mu_B B_0^2/\hbar|\dot{B}_z|$. Here η is a dimensionless measure of the adiabaticity of the field sweep process. We emphasize that β shows monotonic behavior on η. This means that the tilt angle can be deterministically controlled by the transverse field B_0 and the field sweep rate $\dot{B}_z$. In a 2D spin system, a target spin texture $\beta(x, y)$ can be generated by tailoring the spatial distribution of $\vec{B}_0(x, y)$ for a given field sweep process.

2.2. Skyrmion spin texture with a quadrupole magnetic field

Figure 1(c) illustrates how to imprint a Skyrmion spin texture on a 2D atomic condensate by using a 3D quadrupole magnetic field. The quadrupole magnetic field is given as $\vec{B}(r, z) = B'r\hat{r} + (B_z - 2B'z)\hat{z}$ and the zero-field center is located at $z_0 = B_z/2B'$. By linearly sweeping the uniform bias field B_z, we move the zero-field point through the sample placed on the $z = 0$ plane so that a local spin in the sample experiences a field rotation by π as in the previous example. The local adiabaticity of the field sweep process varies over the sample as $\eta(r) = \mu B'^2 r^2/\hbar|\dot{B}_z|$. Ignoring the effects due to the translational motion of atoms and atom–atom interactions, the resultant spatial distribution of the spin direction of the condensate would be

$$\vec{s}(r, \phi) = \cos\beta(r)\hat{z} + \sin\beta(r)(\cos\gamma(r)\hat{r} + \sin\gamma(r)\hat{\phi}), \tag{2}$$

where $\beta(r)$ monotonically increases from $\beta(0) = 0$ to $\beta(\infty) = \pi$. Here $\gamma(r)$ is the azimuthal angle due to the precession accumulated during the field sweep process.

The local spin continuously rotates to the opposite direction from the far-field uniform spin and this is a Skyrmion spin texture. This structure is topologically protected in the $O(3)$ spin space and its topological charge is defined as

$$Q = \frac{1}{4\pi}\int \mathrm{d}x\,\mathrm{d}y\ \vec{s}\cdot(\partial_x\vec{s}\times\partial_y\vec{s}) = 1, \tag{3}$$

representing the number of times the spin texture encloses the whole spin space. Note that the topological charge is independent of γ.

2.3. The polar phase versus the ferromagnetic phase of spin-1 condensates

We consider a Bose–Einstein condensate of spin-1 atoms, whose order parameter can be written as $\Psi = (\psi_1, \psi_0, \psi_{-1})^{\mathrm{T}} = \sqrt{n}\,\mathrm{e}^{\mathrm{i}\vartheta}\zeta$, where $\psi_{0,\pm1}$ is the $|m_z = 0, \pm1\rangle$ component of the order parameter, n is the atomic number density, ϑ is the superfluid phase and ζ is a three-component spinor. The ground state of the spinor condensate at zero magnetic field is determined by the spin-dependent interactions whose energy density is given as $E = \frac{c}{2}n^2|\langle\mathbf{F}\rangle|^2$, where $c = 4\pi\hbar^2(a_2 - a_0)/3m$ (a_F is the two-body s-wave scattering length in the total spin F channel and m is the atomic mass) and $\mathbf{F}$ is the 3×3 Pauli spin matrices. The ground state is polar, i.e. $|\langle\mathbf{F}\rangle| = 0$, for $c > 0$ (e.g. ^{23}Na [17]), or ferromagnetic, i.e. $|\langle\mathbf{F}\rangle| = 1$, for $c < 0$ (e.g. ^{87}Rb [18]).

Here we study the spin textures created with two initial, uniform spin textures: $\zeta = (0, 1, 0)^{\mathrm{T}}$ and $\zeta = (0, 0, 1)^{\mathrm{T}}$, corresponding to the polar and ferromagnetic phases, respectively.

Under the field sweep process, the local spinors of the condensate rotate in the same manner as $\vec{s}$ in equation (2), resulting in

$$\zeta_{\text{polar}}(r,\phi) = \exp(-\mathrm{i}\mathbf{F}\cdot\hat{n}\beta)\begin{pmatrix}0\\1\\0\end{pmatrix} = \begin{pmatrix}-\frac{1}{\sqrt{2}}\mathrm{e}^{-\mathrm{i}\phi}\sin\beta(r)\\ \cos\beta(r)\\ \frac{1}{\sqrt{2}}\mathrm{e}^{\mathrm{i}\phi}\sin\beta(r)\end{pmatrix} \tag{4}$$

and

$$\zeta_{\text{ferro}}(r,\phi) = \exp(-\mathrm{i}\mathbf{F}\cdot\hat{n}\beta)\begin{pmatrix}0\\0\\1\end{pmatrix} = \begin{pmatrix}\mathrm{e}^{-\mathrm{i}2\phi}\sin^2\frac{\beta(r)}{2}\\ \frac{1}{\sqrt{2}}\mathrm{e}^{-\mathrm{i}\phi}\sin\beta(r)\\ \cos^2\frac{\beta(r)}{2}\end{pmatrix}, \tag{5}$$

where $\hat{n}(\phi) = -\hat{x}\sin\phi + \hat{y}\cos\phi$ is the axis of the local field rotation and we omit the precession angle $\gamma(r)$ that is not important for characterizing the spin textures. Because of the ϕ dependence of the rotation axis, the Berry phase factor of $\mathrm{e}^{\mathrm{i}(m_{\mathrm{F}}-m_z)\phi}$ [19] develops, leading to the phase winding numbers of (−1,0,1) and (−2, −1,0) for the $|m_z = +1, 0, -1\rangle$ components in the polar ($m_{\mathrm{F}} = 0$) and ferromagnetic ($m_{\mathrm{F}} = -1$) phases, respectively. The total angular momentum of the condensate is preserved to be zero for the polar phase but, in contrast, changes for the ferromagnetic phase [20].

Although these two final states are identical to each other in terms of spin pattern, their topological characteristics are fundamentally different. The symmetry of the order parameter space of the polar phase is $M_{\text{polar}} = (U(1)\times S^2)/\mathbb{Z}_2$ where $U(1)$ is for the gauge symmetry of the superfluid phase, S^2 is for the rotational symmetry of the spinor and $\mathbb{Z}_2$ comes from the invariant symmetry under $\vec{n}\to-\vec{n}$ and $\vartheta\to\vartheta+\pi$ [21]. Since the second homotopy group $\pi_2(M_{\text{polar}}) = \mathbb{Z}$ is not trivial, topologically stable 2D Skyrmions exist in the polar phase, so ζ_{polar} represents a 2D Skyrmion excitation [22]. On the other hand, the order parameter of the ferromagnetic phase has $SO(3)$ symmetry and the second homotopy group $\pi_2(SO(3)) = 0$, meaning that the Skyrmion spin texture is not topologically protected [23]. The spin excitation ζ_{ferro} in the ferromagnetic phase is referred to as the Anderson–Toulouse vortex [24]. When $\beta(r\to\infty) = \pi/2$, we refer to ζ_{polar} as a coreless spin vortex because it has only a spin flow with no net mass flow [23] and ζ_{ferro} as the Mermin–Ho vortex [25]. The Anderson–Toulouse and Mermin–Ho vortices have been studied in superfluid He-3 systems [26, 27]. Recent theoretical studies showed that these coreless vortex states are the ground states of ferromagnetic spinor condensates under slow rotation [28, 29].

3. Experimental results

3.1. The creation of Skyrmion spin textures in trapped condensates

We perform the spin texture imprinting experiments with $F = 1$ ^{23}Na condensates as described in [22]. A pancake-shaped, quasi-pure condensate is prepared in a 1064 nm optical dipole trap with trapping frequencies of $\omega_{x,y,z} = 2\pi\times(3.5, 4.6, 430)$ Hz. With a typical atom number of $\approx 1.2\times10^6$, the transverse Thomas–Fermi radii of the trapped condensate are $(R_x, R_y)\approx(150, 120)\,\mu$m and the atomic peak density $n\approx 1.2\times10^{13}\,\mathrm{cm}^{-3}$. The spin healing length $\xi_{\mathrm{s}} = \hbar/\sqrt{2mcn}\approx 6.4\,\mu$m ($a_2 - a_0 \simeq 5.7a_{\mathrm{B}}$ and a_{B} is the Bohr radius [30]) is much larger than the thickness of the condensate $\approx 1\,\mu$m, so our sample is an effective 2D spin system.

The condensate is initially generated in the $|m_F = -1\rangle$ state [31]. For the study of the spin textures of the polar phase, a full population transfer to the $|m_F = 0\rangle$ state is made before applying a spin texture imprinting process, using an adiabatic Landau–Zener RF sweep at a uniform bias field of $B_z = 20\,\mathrm{G}$, where the quadratic Zeeman shift is about 0.1 MHz.

The magnetic field for the spin texture imprinting is provided by three pairs of coaxial coils: one is for the quadrupole field and the others are for the uniform bias field to the $\pm z$-directions, respectively. We adiabatically turn on the quadrupole field to $B' = 7\,\mathrm{G\,cm^{-1}}$ in 3.5 ms with $B_z = 2\,\mathrm{G}$ and rapidly ramp the axial bias field to $B_z < -1\,\mathrm{G}$ at a variable rate $\dot{B}_z$. Then we switch off the quadrupole field within $150\,\mu$s and stabilize the bias field to $B_z = -500\,\mathrm{mG}$ within $100\,\mu$s. The quadrupole field provides an additional, transverse (anti-)trapping potential to atoms in the $|m_z = -1(1)\rangle$ state, so it would induce breathing-mode excitations for the field sweep process. To reduce this deleterious effect, we shortened the turn-on time of the quadrupole field as much as possible without losing the adiabaticity of the field change. During the imprinting process, the radial size of the condensate initially prepared in the $|m_z = -1\rangle$ state was observed to change by less than 3%, so the mechanical perturbation was negligible.

The density distributions $n_{0,\pm1}$ of the $|m_z = 0, \pm1\rangle$ components are measured by taking an absorption image after the Stern–Gerlach separation [22]. After the field sweep, we switch off the optical trap and apply a magnetic field gradient for 6 ms to spatially separate the spin components in the x-direction. An absorption image is taken using the $|F = 2\rangle \rightarrow |F' = 3\rangle$ cycling transition after pumping the atoms into the $|F = 2\rangle$ state. For a 15 ms time-of-flight, the condensate expands by about 10% in the transverse direction.

In order to characterize the spin textures, we reconstruct the distribution of the tilt angle $\beta(x, y)$ from the measured density distributions using the relations $\cos^2\beta = n_0/(n_1 + n_0 + n_{-1})$ and $\cos\beta = (n_1 - n_{-1})/(n_1 + n_0 + n_{-1})$ for the polar and ferromagnetic phases, respectively (see equations (4) and (5)). Figure 2 displays the typical spin textures observed in the condensates. The tilt angle clearly shows radial symmetry and monotonically increases from the center to the boundary of the condensate as expected. The tilt angle at the sample boundary could be controlled with the field sweep rate and we observed 2D Skyrmions and the coreless spin vortex states with the polar phase, and the Anderson–Toulouse and Mermin–Ho vortex states with the ferromagnetic phase. The phase winding nature of the spin textures has been confirmed in previous experiments by measuring the quadrupole oscillation frequencies [9], observing the splitting of a doubly charged vortex core [14] and matter wave interference patterns between the spin components [22].

3.2. Characterization of the spin texture imprinting method

The magnetic field sweep was performed very rapidly within a few hundreds of μs. Since this time scale is too short for the dynamics due to atom–atom interactions to be involved, we expect that the spin tilt angle $\beta(x, y)$ might be fully determined by the local adiabaticity $\eta(x, y)$ of the field rotation, which we found to be the case. Figure 3 shows $\cos^2\beta(\eta)$ obtained by azimuthally averaging $\cos^2\beta(x, y)$ and $\cos\beta(x, y)$ of the polar and ferromagnetic spin textures, respectively. We estimate the local adiabaticity as $\eta(r) = (\mu_B/2)B'^2(\kappa r)^2/\hbar|\dot{B}_z|$ with $\kappa = 0.9$ to account for the transverse expansion due to the time-of-flight, which is an oversimplification of the expansion dynamics. Remarkably, the data from the four different spin textures, regardless of the phase of the sample, overlap nicely and, furthermore, show good quantitative agreement with the numerical calculation for a single spin. This observation clearly demonstrates that with

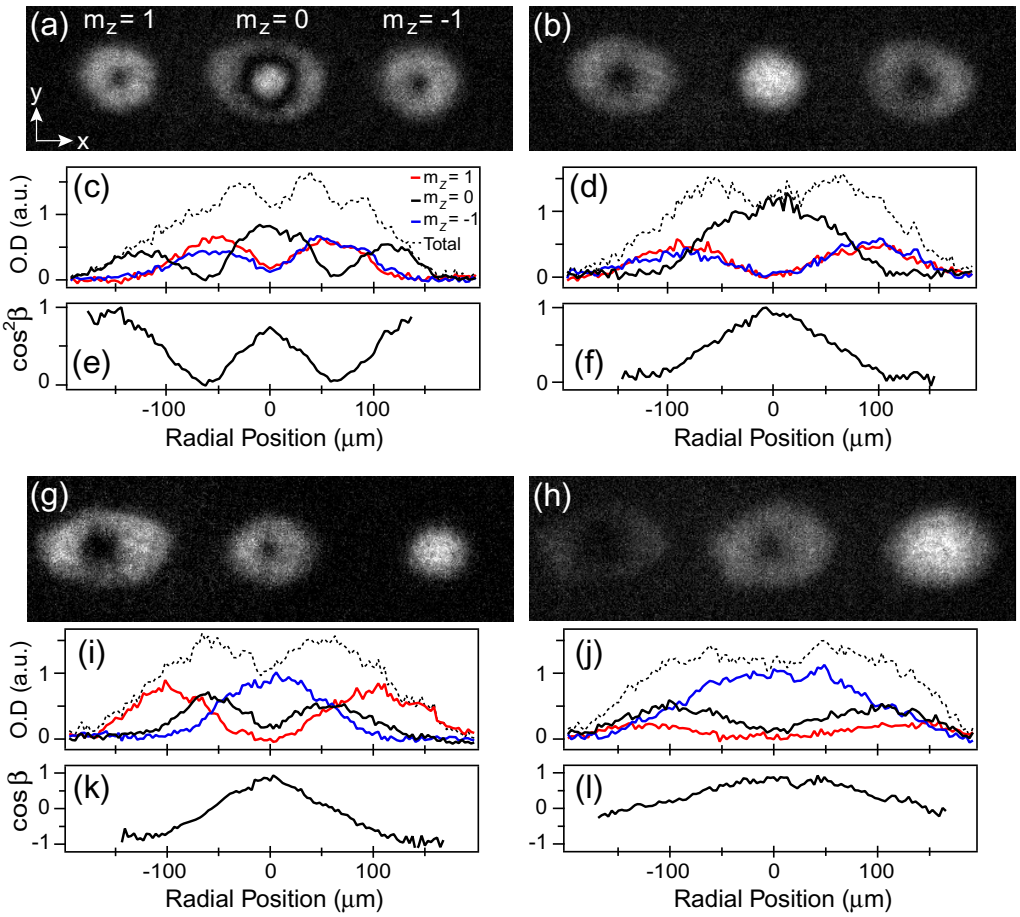

Figure 2. Skyrmion spin textures in spin-1 Bose–Einstein condensates. Skyrmion spin textures were imprinted with the field rotation method in trapped condensates that were initially prepared in (a, b) the $|m_z = 0\rangle$ (polar) or (g, h) $|m_z = -1\rangle$ (ferromagnetic) state. Density distributions of the three spin components, measured after a Stern–Gerlach spin separation, represent (a) a 2D Skyrmion, (b) a coreless spin vortex, (g) the Anderson–Toulouse vortex and (h) the Mermin–Ho vortex. The quadrupole field gradient was $B' = 7\,\mathrm{G\,cm^{-1}}$ and the field ramp rate was (a) $|\dot{B}_z|$ =10, (b) 46, (g) 10 and (h) $35\,\mathrm{G\,ms^{-1}}$. Panels (c, d, i, j) display the central cuts of the optical densities of the spin components along the x-direction and (e, f, k, l) show the corresponding tilt angle distributions $\beta(x)$ (see text). The field of view in the images is 1.3 mm × 390 μm.

this field rotation method the spin textures are generated in a controllable and deterministic manner. We infer that the expansion dynamics during the time-of-flight does not significantly modify the spin textures in our experimental conditions, ensuring that the measured density distributions adequately reveal the *in situ* distributions.

3.3. The creation of highly charged Skyrmions

One can envisage the creation of highly charged, i.e. $Q > 1$, Skyrmion spin textures by applying the imprinting process multiple times to a trapped sample. We explored this possibility with

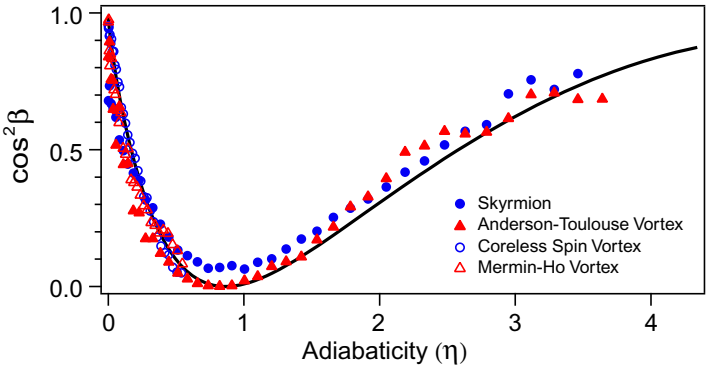

Figure 3. Spin tilt angle versus adiabaticity of the field rotation. The data points are obtained from the four different spin textures: the 2D Skyrmion (solid circle), the Anderson–Toulouse vortex (solid triangle), the coreless spin vortex (open circle) and the Mermin–Ho vortex (open triangle). The solid line is from the numerical calculation.

an experimental sequence with two consecutive field sweeps as described in figure 4. It is important to note that the additional tilt angle β_2 from the second field sweep depends not only on the adiabaticity of the field sweep but also on both the initial tilt angle β_1 and the azimuthal angle γ after the first field sweep. Moreover, γ keeps evolving in the interim between the two field sweeps. Although we know that it is possible to trace the evolution of the spin texture for a short time scale, precise control of the trajectory of the magnetic field would be technically demanding.

Reasoning that the dependence of β_2 on γ decreases when β_1 is close to zero or π, we adopted a more reliable scheme where the ratio of the local adiabaticities of the two field sweeps $\eta_2/\eta_1 \ll 1$ so that the first Skyrmion spin texture would be almost intact for the second field sweep process. In other words, the second field sweep creates an additional spin bending structure in the outer region of the first Skyrmion. Figure 4(a) illustrates the control sequence of the magnetic field. First, we imprinted a Skyrmion spin texture with $B' = 9.4\,\mathrm{G\,cm^{-1}}$ and $|\dot{B}_z| = 12\,\mathrm{G\,ms^{-1}}$ [$\eta(R_x) = 7.3$] in a polar condensate, resulting in a small, but distinguishable density-depletion ring in the $|m_z = 0\rangle$ component (figure 4(c)). Within 5 ms, we abruptly changed the field direction and applied the second field sweep with $B' = 7.0\,\mathrm{G\,cm^{-1}}$ and $|\dot{B}_z| = 40\,\mathrm{G\,ms^{-1}}$ [$\eta(R_x) = 1.2$]. Figure 4(d) shows the final spin texture where a double-ring structure is observed in all the spin components, indicating $Q > 1$.

4. Summary and outlook

In conclusion, we have investigated the magnetic field rotation method for imprinting Skyrmion spin textures in spin-1 Bose–Einstein condensates and demonstrated the creation of 2D Skyrmions and various coreless vortices in the polar and ferromagnetic phases. The spatial distributions of the spin textures show good quantitative agreement with the local single-spin description, where the spin tilt angle is fully determined by the local adiabaticity of the field rotation. This observation indicates that deterministic imprinting of spin textures is possible using this field rotation method. Furthermore, we have demonstrated the first creation of $Q > 1$ Skyrmion spin textures by consecutively applying the imprinting process multiple times to a trapped condensate.

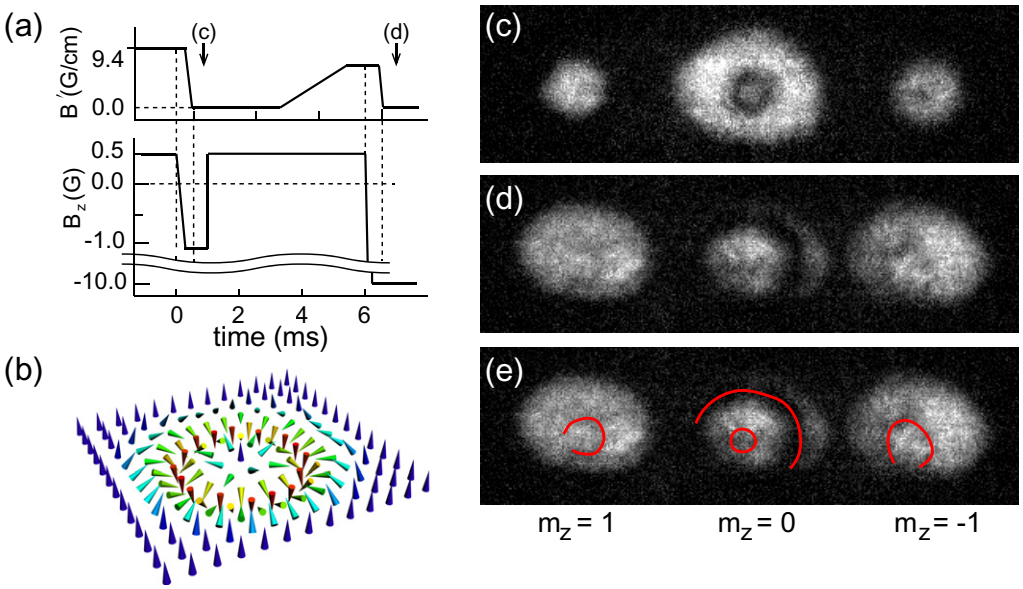

Figure 4. The creation of highly charged Skrymions in a spinor condensate. A Skyrmion spin texture with $Q > 1$ is generated by consecutively applying the imprinting process twice. (a) The control sequence of the magnetic field. (b) 3D illustration of a $Q = 2$ Skyrmion spin texture. Density distributions of the spin components after (c) the first and (d) the second field sweep, respectively. (e) The same as (d) with guidelines for the density-depleted regions.

Since the sample is kept in the optical trap after the spin texture imprinting process, our current experimental setup provides immediate opportunities to study the dynamic stabilities of the 2D Skyrmions and the coreless vortices. Recent theoretical studies showed that the Anderson–Toulouse and Mermin–Ho coreless vortices are dynamically unstable toward vortex splitting and phase separation [32]. We expect that this technique can be extended to engineer 3D topological excitations with timely control of the magnetic field. It has been proposed that knots [4] or Dirac monopole structures [5] can be generated by placing the zero-field point of a quadrupole field in a 3D condensate.

Acknowledgments

This work was supported by the National Research Foundation of Korea (NRF) grants funded by the Korean Government (MEST) (numbers 2010-0010172, 2011-0017527, 2008-0062257 and WCU-R32-10045). JC acknowledges support from a Global PhD Fellowship.

References

[1] Leonhardt U and Volovik G E 2000 How to create an Alice string in a vector Bose–Einstein condensate *JETP Lett.* **72** 46

[2] Khawaja U A and Stoof H 2001 Skyrmions in a ferromagnetic Bose–Einstein condensate *Nature* **411** 918

[3] Ruostekoski J and Anglin J R 2003 Monopole core instability and Alice rings in spinor Bose–Einstein condensates *Phys. Rev. Lett.* **91** 190402

[4] Kawaguchi Y, Nitta M and Ueda M 2008 Knots in a spinor Bose–Einstein condensate *Phys. Rev. Lett.* **100** 180403
[5] Pietilä V and Möttönen M 2009 Creation of Dirac monopoles in spinor Bose–Einstein condensates *Phys. Rev. Lett.* **103** 030401
[6] Madison K W, Chevy F, Wohlleben W and Dalibard J 2000 Vortex formation in a stirred Bose–Einstein condensate *Phys. Rev. Lett.* **84** 806
[7] Matthews M R, Anderson B P, Haljan P C, Hall D S, Wieman C E and Cornell E A 1999 Vortices in a Bose–Einstein condensate *Phys. Rev. Lett.* **83** 2498
[8] Andersen M F, Ryu C, Cladè P, Natarajan V, Vaziri A, Helmerson K and Phillips W D 2006 Quantized rotation of atoms from photons with orbital angular momentum *Phys. Rev. Lett.* **97** 170406
[9] Leanhardt A E, Görlitz A, Chikkatur A P, Kielpinski D, Shin Y, Pritchard D E and Ketterle W 2002 Imprinting vortices in a Bose–Einstein condensate using topological phases *Phys. Rev. Lett.* **89** 190403
[10] Bretin V, Rosenbusch P, Chevy F, Shlyapnikov G V and Dalibard J 2003 Quadrupole oscillation of a single-vortex Bose–Einstein condensate: evidence for Kelvin modes *Phys. Rev. Lett.* **90** 100403
[11] Coddington I, Engels P, Schweikhard V and Cornell E A 2003 Observation of Tkachenko oscillations in rapidly rotating Bose–Einstein condensates *Phys. Rev. Lett.* **91** 100402
[12] Neely T W, Samson E C, Bradley A S, Davis M J and Anderson B P 2010 Observation of vortex dipoles in an oblate Bose–Einstein condensate *Phys. Rev. Lett.* **104** 160401
[13] Freilich D V, Bianchi D M, Kaufman A M, Langin T K and Hall D S 2010 Real-time dynamics of single vortex lines and vortex dipoles in a Bose–Einstein condensate *Science* **329** 1182
[14] Shin Y, Saba M, Vengalattore M, Pasquini T A, Sanner C, Leanhardt A E, Prentiss M, Pritchard D E and Ketterle W 2004 Dynamical instability of a doubly quantized vortex in a Bose–Einstein condensate *Phys. Rev. Lett.* **93** 160406
[15] Leanhardt A E, Shin Y, Kielpinski D, Pritchard D E and Ketterle W 2003 Coreless vortex formation in a spinor Bose–Einstein condensate *Phys. Rev. Lett.* **90** 140403
[16] Leslie L S, Hansen A, Wright K C, Deutsch B M and Bigelow N P 2009 Creation and detection of Skyrmions in a Bose–Einstein condensate *Phys. Rev. Lett.* **103** 250401
[17] Stenger J, Inouye S, Stamper-Kurn D M, Miesner H-J, Chikkatur A P and Ketterle W 1998 Spin domains in ground-state Bose–Einstein condensates *Nature* **396** 345
[18] Chang M S, Hamley C D, Barrett M D, Sauer J A, Fortier K M, Zhang W, You L and Chapman M S 2004 Observation of spinor dynamics in optically trapped ^{87}Rb Bose–Einstein condensates *Phys. Rev. Lett.* **92** 140403
[19] Berry M V 1984 Quantal phase factors accompanying adiabatic changes *Proc. R. Soc.* A **392** 45
[20] Isoshima T, Nakahara M, Ohmi T and Machida K 2000 Creation of a persistent current and vortex in a Bose–Einstein condensate of alkali-metal atoms *Phys. Rev.* A **61** 063610
[21] Mukerjee S, Xu C and Moore J E 2006 Topological defects and the superfluid transition of the $s = 1$ spinor condensate in two dimensions *Phys. Rev. Lett.* **97** 120406
[22] Choi J, Kwon W J and Shin Y 2012 Observation of topologically stable 2D Skyrmions in an antiferromagnetic spinor Bose–Einstein condensate *Phys. Rev. Lett.* **108** 035301
[23] Ueda M and Kawaguchi Y 2010 Spinor Bose–Einstein condensates arXiv:1001.2072
[24] Anderson P W and Toulouse G 1977 Phase slippage without vortex cores: vortex textures in superfluid ^{3}He *Phys. Rev. Lett.* **38** 508
[25] Mermin N D and Ho T-L 1976 Circulation and angular momentum in the a phase of superfluid helium-3 *Phys. Rev. Lett.* **36** 594
[26] Salomaa M M and Volovik G E 1987 Quantized vortices in superfluid 3He *Rev. Mod. Phys.* **59** 533
[27] Blaauwgeers R, Eltsov V B, Krusius M, Ruohio J J, Schanen R and Volvik G E 2000 Double-quantum vortex in superfluid 3He-A *Nature* **404** 471
[28] Mizushima T, Machida K and Kita T 2002 Mermin–Ho vortex in ferromagnetic spinor Bose–Einstein condensates *Phys. Rev. Lett.* **89** 030401

[29] Martikainen J P, Collin A and Suominen K A 2002 Coreless vortex ground state of the rotating spinor condensate *Phys. Rev.* A **66** 053604

[30] Burke J P, Greene C H and Bohn J L 1998 Multichannel cold collisions: simple dependences on energy and magnetic field *Phys. Rev. Lett.* **81** 3355

[31] Heo M S, Choi J and Shin Y 2011 Fast production of large ^{23}Na Bose–Einstein condensates in an optically plugged magnetic quadrupole trap *Phys. Rev.* A **83** 013622

[32] Takahashi M, Pietilä V, Möttönen M, Mizushima T and Machida K 2009 Vortex-splitting and phase-separating instabilities of coreless vortices in $F = 1$ spinor Bose–Einstein condensates *Phys. Rev.* A **79** 023618